The EMBO Journal vol.5 no.3 pp.529–534, 1986

Three-dimensional structure of clathrin cages in ice

G.P.A.Vigers, R.A.Crowther and B.M.F.Pearse

Medical Research Council, Laboratory of Molecular Biology, Hills Road, Cambridge CB2 2QH, UK

Communicated by R.A.Crowther

We have collected tilt series of electron micrographs from unstained clathrin cages embedded in vitreous ice. From these micrographs we have generated three-dimensional reconstructions of individual hexagonal barrels, which show details of the internal structure. Four types of preparation have been examined: (i) coated vesicles; (ii) cages reassembled from clathrin heavy and light chains; (iii) reassembled cages treated with elastase to remove the light chains; and (iv) reassembled cages treated with trypsin to remove the light chains and the terminal domains of the clathrin heavy chains. In the intact and elastase-treated cages, the clathrin extends from the vertices into the interior of the polyhedron and forms an inner shell of material. Limited digestion with trypsin removes the inner shell, which indicates that this material corresponds to the terminal domains of the clathrin heavy chains.

Key words: clathrin cages/frozen hydrated specimens/image reconstruction

Introduction

Clathrin forms the polyhedral cage of coated vesicles, which mediate the transfer of selected membrane components within eukaryotic cells (Pearse and Bretscher, 1981). Clathrin cages and coated vesicles have been extensively studied by electron microscopy of negatively-stained preparations (Crowther *et al.*, 1976) and shadowed specimens (Heuser, 1980). The gross morphology of the outer part of the polyhedral coat is now established and some features of the packing of clathrin trimers into the coat have also been described (Crowther and Pearse, 1981). However these studies have not revealed any internal details. The structural role of the 100 kd/50 kd accessory coat proteins (Zaremba and Keen, 1983; Pearse and Robinson, 1984) and the interactions of the coat with the enclosed membrane are unclear. Furthermore the terminal domains of the clathrin heavy chains (Ungewickell *et al.*, 1982; Schmid *et al.*, 1982) are unacounted for, though they are presumed to be located internally (Kirchhausen and Harrison, 1984).

Electron microscopy of unstained frozen hydrated specimens provides a means of addressing these problems. Although negative staining and shadowing give good results in mapping the external shape of many specimens, it was recognised some time ago (Taylor and Glaeser, 1974) that considerable advantages might accrue from a technique which froze the specimen in a hydrated state, though the procedures available at that time were difficult to use routinely. The specimens examined in this study were produced by the improved preparation techniques now available (Dubochet *et al.*, 1982), that trap the specimen in a stable layer of vitrified water. Such specimens are sufficiently transparent that internal details of the structure can be visualised, but are much more radiation sensitive than negatively-stained or shadowed preparations. Previous processing of images of frozen hydrated specimens has therefore depended on combining data from separate crystalline areas (Unwin and Ennis, 1984; Milligan *et al.*, 1984) or on exploiting the helical symmetry of the specimen (Lepault and Leonard, 1985). In this way only a single exposure of a given area needs to be taken in the microscope. However, to reconstruct individual particles of low symmetry, one must collect tilt series, necessitating multiple exposures of a given area. The greatest number of exposures reported by other workers is four (J. Dubochet, personal communication), but by improving the observational procedures we have now collected many tilt and focal series with up to 11 exposures of the same area. This allows three-dimensional reconstructions of individual particles to be computed.

We have calculated maps of reassembled clathrin cages which clearly demonstrate the power of this approach and reveal much internal detail. In particular, under the vertices of the outer polyhedral shell there are inwardly pointing 'fingers' of density, which give rise to an inner shell of material. These fingers are removed by treatment of the cages with trypsin, but not with elastase, and hence can be identified as the terminal domains of the clathrin heavy chains.

Results

Four different types of specimen have been examined: (i) native coated vesicles isolated from human placenta; (ii) cages reassembled from clathrin heavy and light chains which were purified from bovine brain; (iii) reassembled cages treated with elastase to remove the light chains; and (iv) reassembled cages treated with trypsin to remove both light chains and the terminal domains of the heavy chains. As before (Crowther and Pearse, 1981), we use the term cage to denote a closed polyhedral lattice of clathrin heavy and light chains, while the term coat denotes the clathrin cage plus the 100-kd and 50-kd accessory proteins.

Coated vesicles

The general appearance of a coated vesicle preparation, when imaged in the frozen hydrated state, is shown in Figure 1. The images display sharp detail and evidence of internal structure. Characteristic images of previously identified structures are clearly visible, including the 'hexagonal barrel' and 'tennis ball' classes (Crowther *et al.*, 1976). Vesicles can be seen within the larger coats and appear to be well preserved, whereas in negative stain the preservation is poor. Only the larger coats appear to contain vesicles and these show that there is a distance of 21 ± 2 nm between the surface of the vesicle and the outer surface of the surrounding coat.

Although the coated vesicles embedded in vitreous ice are well preserved, the population is very heterogeneous and it is uncertain how much of the accessory proteins a given particle might contain. We therefore decided to use cages reassembled from purified clathrin, without accessory proteins, for image reconstruction. This simplifies interpretation of particular features seen in the reconstructions.

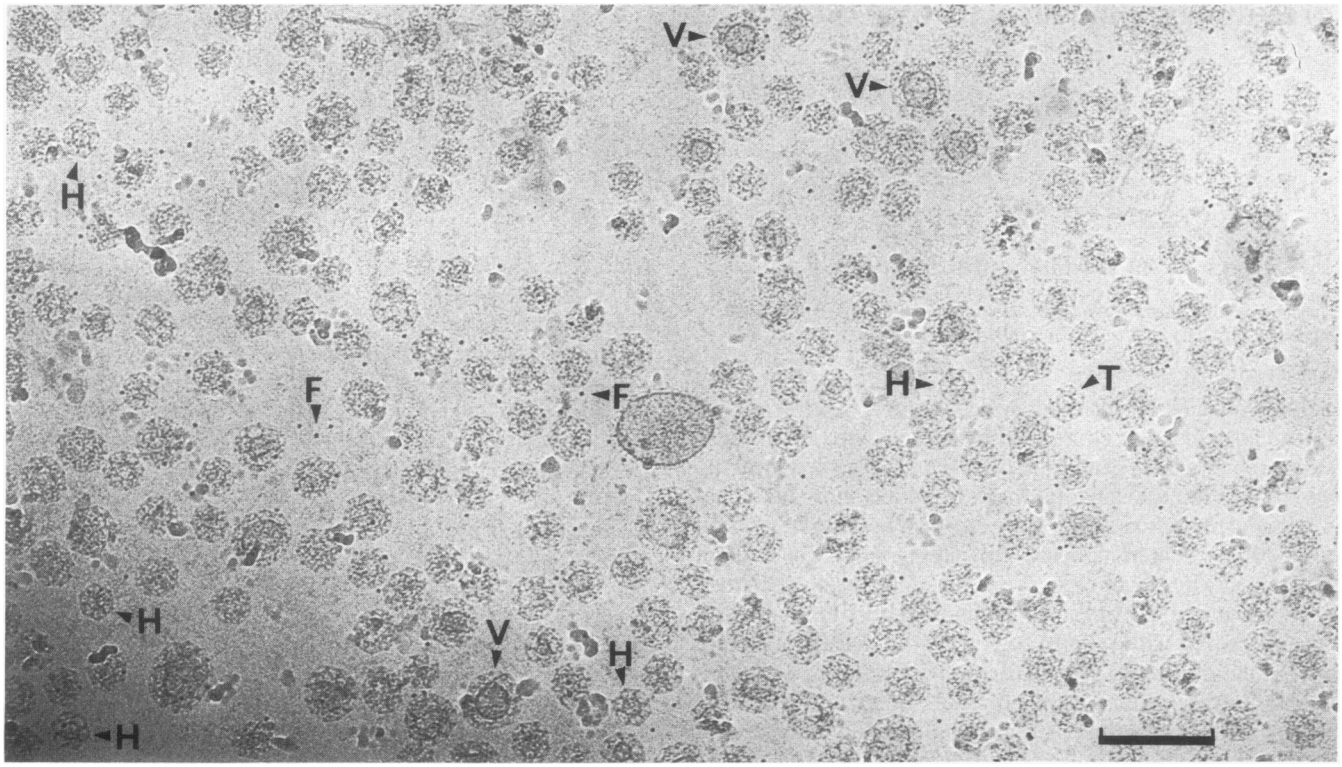

Fig. 1. Field of unstained placental coated vesicles in ice. Hexagonal barrels (H), tennis ball structures (T), larger coats containing vesicles (V) and ferritin (F) are indicated. Scale bar 200 nm.

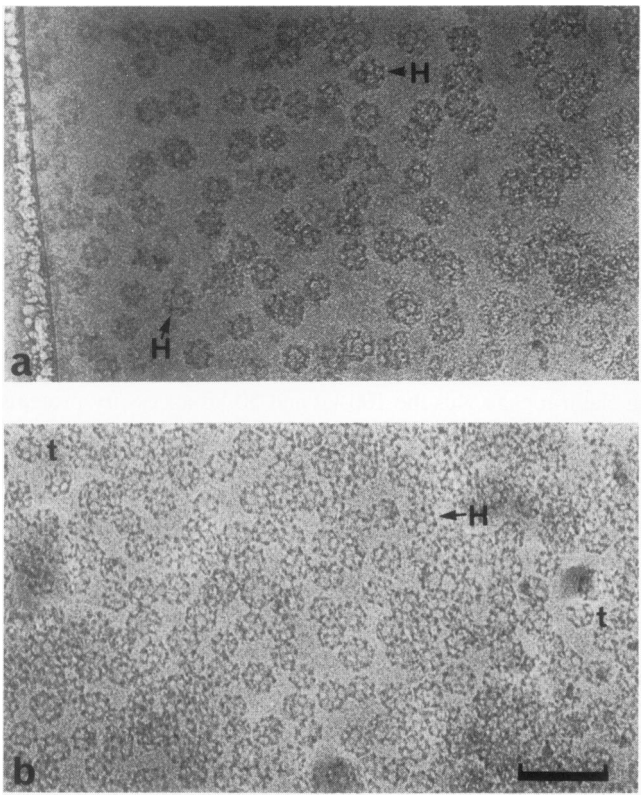

Fig. 2. **(a)** Field of unstained reassembled clathrin cages. This is the eleventh exposure in a tilt series; note that there is bubbling damage on the carbon support film but not around the cages. The image quality deteriorates in very thick ice (left hand edge) or too thin ice (right hand edge). **(b)** Field of unstained reassembled clathrin cages after treatment with trypsin. Many of the same views as in Figure 1 are visible, including hexagonal barrels (H), but examples of small tetrahedral particles (t) are also present. Scale bar 200 nm.

Intact reassembled cages

Figure 2a shows part of a field of reassembled cages and Figure 2b shows part of a field of reassembled cages after limited digestion with trypsin. These images are from the eleventh exposures in their respective tilt series. It can be seen that, although bubbling is evident over the carbon film (left hand side of Figure 2a), the cages still show good structural details. The thickness of the ice varies considerably across the field shown in Figure 2a, being greatest at the left near the carbon film and least on the right. The particles in the thickest ice exhibit poor detail, possibly because of multiple scattering of electrons; the particles in the thinnest ice appear crushed. This emphasises the importance of working with an appropriate thickness of ice. A complete tilt series of a single reassembled cage is shown in Figure 3c, which displays views between $+30°$ and $-30°$. The views change in accordance with the model previously proposed for the hexagonal barrel (Figure 3a).

Figure 4a shows a three-dimensional map of a reassembled cage, based on an average of four independent reconstructions from different tilt series (including the one in Figure 3c), which in addition has been 622 averaged. The 622 averaging and adding has been carried out to reduce the noise level in the maps and to emphasise the common features of high symmetry, for ease of interpretation. The outer polyhedral shell of the reconstructed image agrees well with the qualitative results of previous model building studies based on negatively stained preparations. The puckered boat-shape of the equatorial hexagons (Crowther *et al.*, 1976) is apparent in the $+30°$ view of the reprojected image (Figure 3d) and the skewed arrangement of the holes in the polygonal faces (Crowther and Pearse, 1981) is clear in Figure 4a.

However the map also shows considerable density beneath the outer polyhedral shell. The material apears as 'fingers' of high density, projecting inwards from under the vertices of the cage

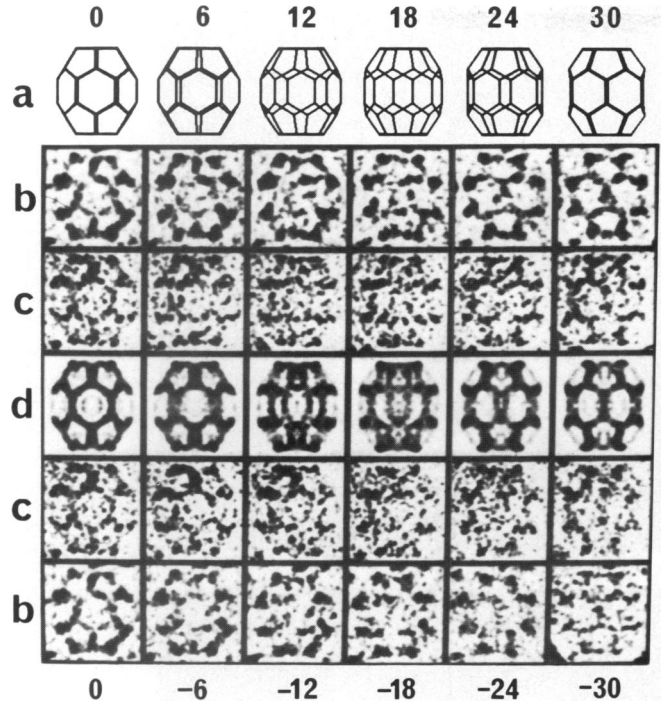

Fig. 3. Tilt series of two hexagonal barrels, with associated gallery of models. The relative angles of view over the range −30° to +30° are indicated. Total accumulated electron dose during each series is 2000 e nm^{-2}. **(a)** Gallery of model views. **(b)** Trypsin-treated reassembled cage, in which the light chains and the terminal domains of the heavy chains have been cleaved. **(c)** Intact reassembled clathrin cage. **(d)** Projections of the reconstructed and averaged map shown in Figure 4a. The projected views are consistent both with the gallery of model views and with the individual tilt series. The assumed 622 symmetry of the barrel means that the images generated by tilting between 0° and +30° will give superposition patterns rotated in the plane by 180° relative to those between 0° and −30°. Thus for the model shown in row **(a)** and the reprojection in row **(d)** only 0° to +30° views are shown.

and running into the central lumen under the polyhedral faces, producing an inner shell of material beneath the outer polyhedron. There appear to be three fingers of density projecting from each vertex and these splay out, with one of the three fingers running under each of the three polygonal faces surrounding a vertex. The fingers, seen most clearly when viewing the reconstruction from the inside as in Figure 4c,d, come together to make a ring of density beneath the hole in each polygonal face.

The overall thickness of the outer and inner shells in the reconstruction is ~ 18 nm, as can be seen in the plot of the radial density function (Figure 5). The overall height of the reconstructed barrel is 71 ± 3 nm. The length of the individual edges from vertex to vertex is 18.4 ± 0.7 nm, in excellent accord with the previous measurements from negatively-stained fragments of cages (Crowther and Pearse, 1981). The frozen hydrated particle is likely to have its native dimensions and measuring the reconstruction ensures that the edges are not fore-shortened by obliquity. The microscope magnification was calibrated by mixing T4 phage (tail length 110 nm from collar to baseplate) with the clathrin cages before freezing.

Elastase- and trypsin-treated cages

The reconstruction from elastase-treated reassembled cages, which lack the light chains, shows no obvious differences from that of the intact cage. In particular the projecting fingers of density are still present. The radial density function (Figure 5) is similar to that of the intact cage, though the peak corresponding to the inner shell appears slightly reduced. It is not clear whether this is significant, since the light chains are associated with the proximal regions of the clathrin heavy chains (Ungewickell *et al.*, 1982; Ungewickell, 1983; Kirchhausen *et al.*, 1983) and would thus be expected to contribute density to the outer polyhedron. Their removal does not seem to produce differences in the outer shell large enough to be detected at this level of imaging.

After limited trypsin digestion of cages, two similar fragments of the heavy chain of ~110 and 115 kd remain assembled in the familiar polyhedral structure (Schmid *et al.*, 1982; Ungewickell *et al.*, 1982). A field of such particles is shown in Figure 2b and Figure 4b shows our reconstruction of the trypsinized hexagonal barrel. The map was again produced by averaging four reconstructions from different tilt series, including the one shown in Figure 3b, and has again been 622 averaged. It is clear that this map is much emptier than the one from the intact cages (Figure 4a) and lacks the fingers of density seen in the intact cage and in the elastase-treated cage. In the plot of the radial density function (Figure 5), the secondary peak that occurs just inside the main peak in intact and elastase-treated cages is now missing. SDS-polyacrylamide gels of the trypsin-treated cages indicate that the terminal domains of the heavy chains have been cleaved and the light chains removed (data not shown). The terminal domains of the clathrin heavy chains (Ungewickell *et al.*, 1982; Schmid *et al.*, 1982; Kirchhausen and Harrison, 1984) must therefore form the inner structure observed in intact and elastase-treated cages.

Discussion

We have succeeded in collecting tilt series of unstained specimens in vitreous ice, allowing reconstructions of individual particles of low symmetry to be made. The specimens thus prepared remain hydrated and are likely to retain their native dimensions. Since the specimen is unstained, the reconstructed maps have the advantage that details are visible within the polyhedral shell, because of the transparency of the ice. Furthermore the features seen are generated objectively by three-dimensional reconstruction, rather than deduced by model building from a gallery of projected views, as in the earlier work.

The results confirm and extend previous observations on the size and geometry of this particular class of clathrin cage, though we expect the results to be valid for all sizes of cage. The 'boat'-shaped equatorial hexagons in the hexagonal barrel were observed in negative-stained specimens (Crowther *et al.*, 1976). The skewed arrangement of the holes in the polygonal faces, which was a feature of the previously proposed packing scheme (Crowther and Pearse, 1981), is also apparent here. The most striking new result is that the clathrin is seen to extend into the interior of the structure and form an inner shell of material, as shown clearly by the computed radial density functions (Figure 5). The results from protease treatment of the cages indicate that this inner shell corresponds to the terminal domains of the clathrin heavy chains. Thus each leg of a triskelion runs from one vertex along two neighbouring polygonal edges, before turning inwards towards the centre of the cage. The three clathrin terminal domains at each vertex splay out in the angles formed by neighbouring polyhedral edges, making rings of density beneath the polygonal faces. It is not yet clear to which triskelion each projecting finger of density is attached. Figure 6 shows a possible packing scheme for the individual clathrin triskelions in the cage. The model is consistent both with previous studies (Crowther and Pearse, 1981;

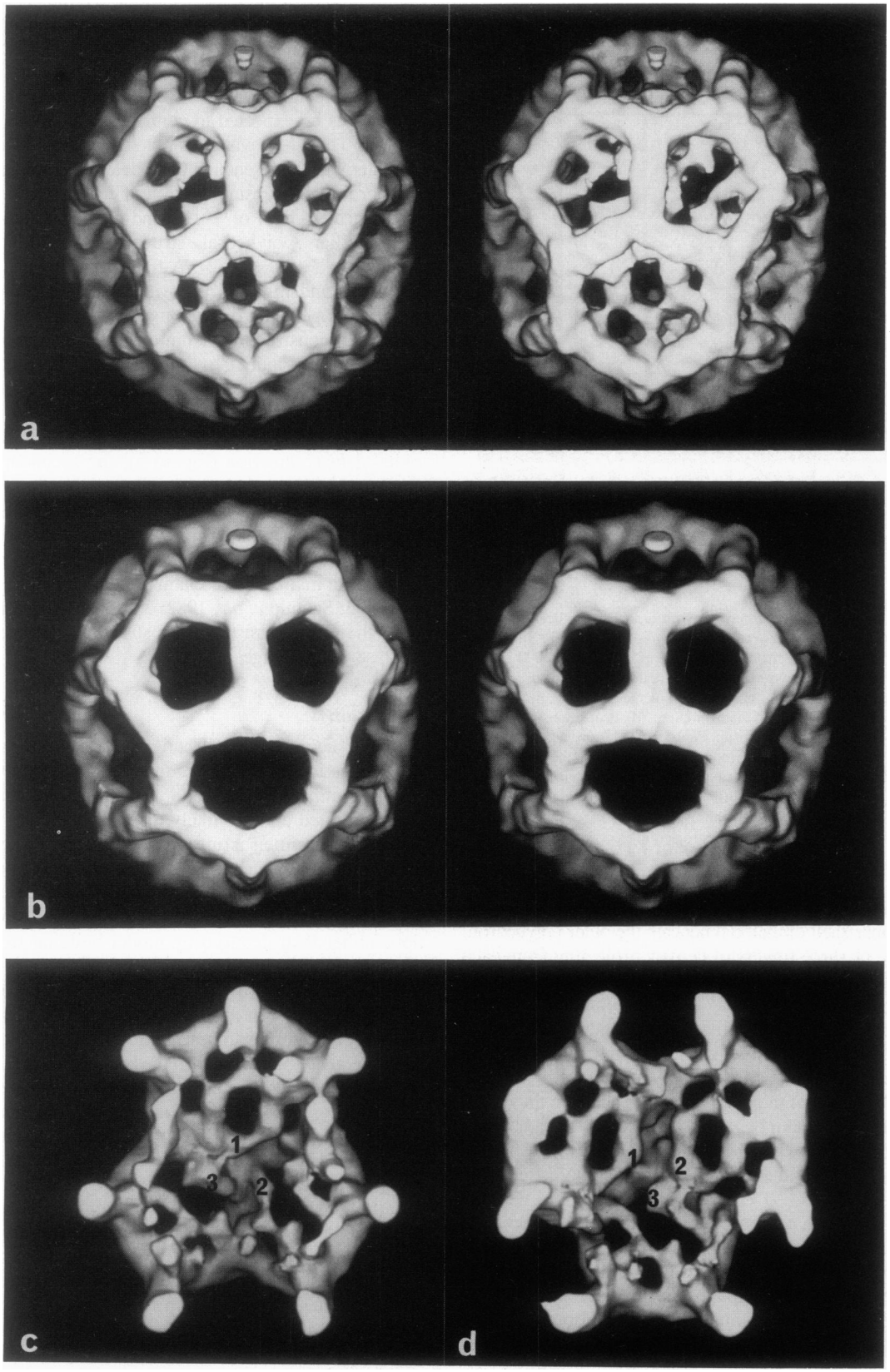

Fig. 4. Reconstructions of hexagonal barrels. Each barrel consists of a hexagon at the top and the bottom, six hexagons around the equator and two rings of six pentagons joining them. **(a)** Stereo-pair of a reconstruction of an intact cage. The angle of display has been chosen to give the clearest view of the interior through two pentagons and an equatorial hexagon. **(b)** Stereo-pair of a reconstruction from trypsin-treated cages, displayed in exactly the same way as **a**. The inwardly projecting fingers of density seen in **(a)** are absent in **(b)**. **(c,d)** Views from inside the cage of part of the reconstruction shown in **a**, showing details of the projecting fingers of density. After averaging, the reconstruction contains three independent classes of vertex and two are shown. **(c)** Shows the vertex between two pentagons and an equatorial hexagon and **(d)** shows the vertex between a pentagon and two equatorial hexagons. In each case the three fingers of density projecting inwards from the vertex are indicated by the labels 1, 2, 3.

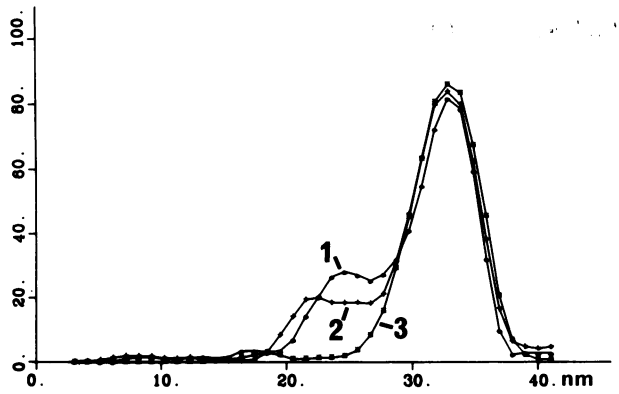

Fig. 5. Plots of density against radius for various reconstructions. **(1)** Intact cage, **(2)** elastase-treated cage **(3)** trypsin-treated cage. The main peak in all curves is centered at 32 nm and represents the density in the outer polyhedron. The shoulders at ~24 nm in intact and elastase-treated cages represent the inner shell of density, which is absent in the trypsin-treated cage. Since the hexagonal barrel is not spherical but has an approximately ellipsoidal shape, map densities were summed in ellipsoidal shells with an eccentricity of 1.1 along the 6-fold axis. The curves show the total mass in each shell, plotted against equatorial radius.

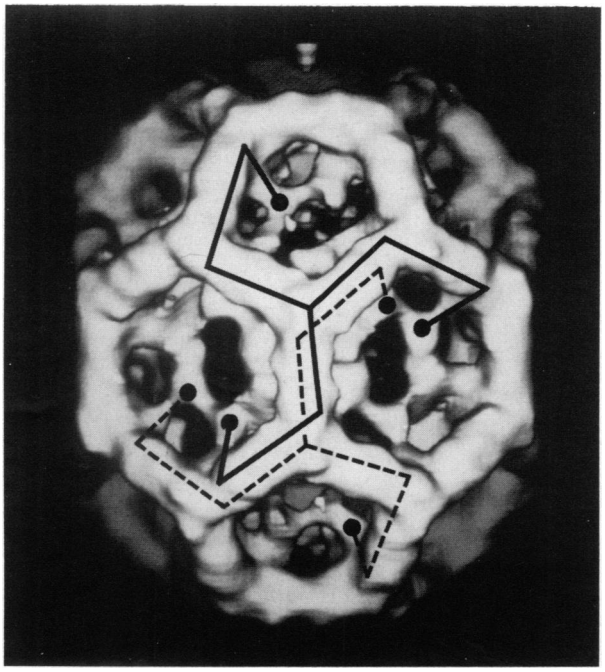

Fig. 6. Proposed packing scheme. Two triskelions centered at the vertices between neighbouring equatorial hexagons have been superimposed diagrammatically on the reconstruction of the intact hexagonal barrel (Figure 4a). Each leg of a triskelion runs from one vertex, along two neighbouring polygonal edges and then turns inwards with its terminal domain forming the inner shell of density seen in the reconstruction.

Kirchhausen and Harrison, 1984) and with the new results reported here.

The overall thickness of material lying outside the surface of the membrane vesicle in coated vesicles (Figure 1) is ~21 nm, in good agreement with that observed in sectioned tissue (Perry and Gilbert, 1979). This is rather greater than the estimated thickness (~18 nm) of the reconstructed clathrin cage. The difference may be significant, since the reassembled cages do not contain the 100 kd/50 kd proteins, which are expected to be present in coated vesicles and which are likely to contribute additional density at inner radii. If the full complement of proteins were present in a hexagonal barrel, the central cavity within would be only ~25 nm diameter, a size barely able to accommodate even the smallest membrane vesicle (Huang, 1969). This may account for the oberved lack of vesicles in the smaller coats (Figure 1). Experiments are now in progress to locate the 100 kd/50 kd proteins in the coat.

Materials and methods

Preparation of clathrin, reassembled cages and coated vesicles

Clathrin was purified from bullock brains as described previously (Pearse and Robinson, 1984). It was reassembled into cages by dialysis against Buffer A [0.1 M MES-NaOH, pH 6.5, 0.2 mM EGTA, 0.5 mM $MgCl_2$, 0.02% NaN_3 and 0.1 mM phenylmethylsulphonyl fluoride (PMSF)]. In such a preparation the cages are very heterogeneous in size. For the electron microscopy a population enriched in barrels was required, so 6 mg of cages (in 1 ml Buffer A) were separated according to size on a 12 ml 5-30% sucrose gradient (in Buffer A) by centrifugation at 80 000 *g* for 1 h at 5°C. The fraction containing the highest percentage of barrels, as judged by electron microscopy of negatively-stained samples, was diluted with an equal volume of Buffer A and the cages concentrated by centrifugation at 100 000 *g* for 1 h at 5°C. The pellet was resuspended in 300 μl of Buffer A.

Treatment of cages with trypsin and elastase was carried out as described by Unanue *et al.* (1981).

Coated vesicles from human placenta were isolated using isotonic gradients (Pearse, 1982).

Electron microscopy

The specimens were prepared on holey carbon grids which had been glow discharged to make them hydrophilic, according to the method of Dubochet *et al.* (1982). Grids were mounted in a Philips PW6591 cold holder, adapted for the Philips EM400 microscope.

The following microscope illumination conditions were used: (i) maximum filament emission; (ii) a 50 μm condenser aperture and a 2 μm spot size for coherent illumination; and (iii) a 20 μm objective aperture to increase the degree of aperture contrast. Tilt series were taken from +30° to −30° in 6° steps, using the Philips low dose system. Images were recorded on Kodak SO 163 electron image film at × 19 500 magnification with a defocus of 6.3 μm, developed in Kodak D19 for 6 min and printed on high contrast paper.

It was found that the cold stage had to be kept scrupulously clean to attain reasonable stability while tilting, and it was necessary to clean the sapphire bearing on the end of the stage before each insertion into the microscope. The thickness of the ice was also found to be critical for good preservation. If the ice was too thick, the images became blurred by excessive multiple and inelastic scattering. If it was too thin, then the particles were seen to be crushed (presumably by surface tension), even when the ice was still thicker than the diameter of the cage (Figure 2a).

The electron dose for each micrograph was estimated from the optical density produced by the direct beam passing through an empty hole in the carbon film, using the figures quoted by Amos *et al.* (1982). The total dose accumulated during each tilt series was ~2000 e nm^{-2}. At the level of detail attained in this study (~5 nm), the particles do not appear to have deteriorated during the exposure series, although bubbling due to radiation damage occurs around aggregates of carbon (Figure 2a) or around the clathrin cages on excessive electron exposure.

Image processing

A biological sample embedded in ice is imaged largely as a weak phase object when the microscope is set up as above, with only a small amount of aperture contrast. Defocal series were taken of cages in ice and these showed that in order to have sufficient contrast in the image a defocus of ~6 μm must be used. Bands of spatial frequencies beyond 1/5 nm^{-1} then contribute to the image with reversed contrast (Thon, 1966), resulting in a defocus fringe at discontinuities of density. From the focal series it was possible to produce a compensated image of the structure (Erickson and Klug, 1971). The details seen in this agreed well with those in the uncompensated and highy defocussed original images. The results from this and other focal series and from computer modelling show that the defocussing does not introduce distortions into the reconstructions described here at the degree of detail presently achieved.

The class of cage chosen for image reconstruction was the 6-fold symmetric hexagonal barrel, previously characterised by negative staining (Crowther *et al.*, 1976). Tilt series were collected from +30° to −30° in 6° steps and the particles to be processed were chosen from large fields (cf. Figure 1), selecting those for which the 6-fold axis lay along the tilt axis. The sampling interval of 6° was chosen to give a reliable resolution of 1/5 nm^{-1} in the reconstruction (Crowther *et al.*, 1970). Collection of 60° of tilt data ensured that the particles selected were indeed hexagonal barrels, and that they had not been significantly flattened

or damaged during preparation or microscopy. Having the 6-fold axis along the tilt axis means that the 60° of data collected are sufficient to make a three-dimensional reconstruction by R-weighted back projection (Gilbert, 1972), provided that the 3-fold sub-symmetry of the cage is used to extend the data to a complete 180° set. The noise in the reconstruction can be further reduced by averaging together reconstructions from different particles and by 622 averaging of the final map, as has been done in the maps presented here. The averaging means that disordered material will be weighted down and so is not seen in the reconstruction.

Images were densitometered with a computer-linked film scanner (Arndt *et al.*, 1969), at a spacing corresponding to 1.1 nm on the specimen. Particles were masked out and aligned using a set of programs written for a VAX 11/780 computer. After three-dimensional reconstruction and averaging, the computed maps were displayed on an AED767 raster graphics terminal, using a surface representation algorithm (Vigers, unpublished).

Acknowledgements

We thank Dr M. Lawrence for writing the computer program for carrying out R-weighted back-projection and C. Villa for assistance with photography. G.P.A.V. held an MRC research studentship during this work.

References

Amos.L.A., Henderson,R. and Unwin,P.N.T. (1982) *Prog. Biophys. Mol. Biol.*, **39**, 183–231.
Arndt,U.W., Barrington-Leigh,J., Mallett,J.F.W. and Twinn,K.E. (1969) *J. Phys. E Ser. 2*, **2**, 385–387.
Crowther,R.A. and Pearse,B.M.F. (1981) *J. Cell Biol.*, **91**, 790–797.
Crowther,R.A., DeRosier,D.J. and Klug,A. (1970) *Proc. R. Soc. Lond.*, **A317**, 319–340.
Crowther,R.A., Finch,J.T. and Pearse,B.M.F. (1976) *J. Mol. Biol.*, **103**, 785–798.
Dubochet,J., Lepault,J., Freeman,R., Berriman,J.A. and Homo,J.C. (1982) *J. Microsc.*, **128**, 219–237.
Erickson,H.P. and Klug,A. (1971) *Phil. Trans. R. Soc. Lond.*, **B261**, 105–118.
Gilbert,P. (1972) *Proc. R. Soc. Lond.*, **B182**, 89–102.
Heuser,J. (1980) *J. Cell Biol.*, **84**, 560–583.
Huang,C. (1969) *Biochemistry*, **8**, 344–352.
Kirchhausen,T. and Harrison,S.C. (1984) *J. Cell Biol.*, **99**, 1725–1734.
Kirchhausen,T., Harrison,S.C., Parham,P. and Brodsky,F.M. (1983) *Proc. Natl. Acad. Sci. USA*, **80**, 2481–2485.
Lepault,J. and Leonard,J. (1985) *J. Mol. Biol.*, **182**, 431–441.
Milligan,R.A., Brisson,A. and Unwin,P.N.T. (1984) *Ultramicroscopy*, **13**, 1–10.
Pearse,B.M.F. (1982) *Proc. Natl. Acad. Sci. USA*, **79**, 451–455.
Pearse,B.M.F. and Bretscher,M.S. (1981) *Annu. Rev. Biochem.*, **50**, 81–101.
Pearse,B.M.F. and Robinson,M.S. (1984) *EMBO J.*, **3**, 1951–1957.
Perry,M.M. and Gilbert,A.B. (1979) *J. Cell Sci.*, **39**, 257–272.
Schmid,S.L., Matsumoto,A.K. and Rothman,J.E. (1982) *Proc. Natl. Acad. Sci. USA*, **79**, 91–95.
Taylor,K.A. and Glaeser,R.M. (1974) *Science*, **186**, 1036–1037.
Thon,F. (1966) *Z. Naturforsch.*, **21a**, 476–478.
Unanue,E.R., Ungewickell,E. and Branton,D. (1981) *Cell*, **26**, 439–446.
Ungewickell,E.E. (1983) *EMBO J.*, **2**, 1401–1408.
Ungewickell,E.E., Unanue,E. and Branton,D. (1982) *Cold Spring Harbor Symp. Quant. Biol.*, **46**, 723–731.
Unwin,P.N.T. and Ennis,P.D. (1984) *Nature*, **307**, 609–613.
Zaremba,S. and Keen,J.H. (1983) *J. Cell Biol.*, **97**, 1339–1347.

Received on 31 December 1985